2026 IEEE International Conference on Robotics and Automation (ICRA 2026)
June 1-5, 2026. Vienna, Austria

Decentralized admittance control for a multi–manipulator system: theory and experiments

Graziano Carriero[1], Monica Sileo[2], Sebastiano Fregnan[3], Francesco Pierri[2], *Member, IEEE*, Fabrizio Caccavale[1], *Senior Member, IEEE*, Yiannis Karayiannidis[3], *Member, IEEE*

***Abstract*— This paper presents a decentralized control framework for cooperative object transportation with multiple robotic manipulators. In particular two admittance schemes are designed in order to regulate external contact wrenches and internal interaction wrenches without a central unit or all-to-all communication. Each manipulator estimates the wrenches exerted by its teammates through a bank of consensus-based observers that exploits a strongly connected communication graph. These estimates feed two local admittance filters: an external filter, computing the reference object trajectory while limiting environmental wrenches, and an internal filter, generating the end-effector trajectory to minimize each robot's contribution to internal wrenches. Experiments carried out with three 7-DOF Franka Emika Panda arms show a marked reduction of both external and internal wrenches, demonstrating the effectiveness and robustness of the proposed approach.**

I. Introduction

Collaboration among multiple robots becomes essential for tasks beyond the capabilities of a single agent, such as transporting large or heavy objects [1]. A common approach is to model all robots and the object within a centralized architecture [2]. For example, [3], [4] address dual-arm manipulation by controlling the relative pose of the arms alongside the absolute position of the object. However, centralized strategies become impractical under limited communication or central unit failures. These issues can be mitigated through decentralized and distributed approaches, which improve scalability and robustness. In leader–follower schemes, one robot defines the object's trajectory while the others track it using compliant control [5]. For tasks such as balancing items on a tray, a Model Predictive Control strategy has been proposed [6], while [7] estimate the object's centroid from relative positions and apply distributed control to achieve cooperative rotation.

Another key challenge is managing the wrenches exchanged between the manipulators and the object-distributing them to reduce individual robot effort while minimizing their impact on the object to preserve its integrity. This can be addressed through impedance and admittance control [8], [9].

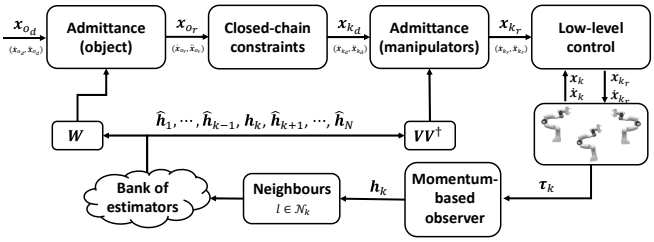

Fig. 1. Block scheme of the overall control architecture for the k-th agent. The bank of estimators enables the distributed information flow among the robots ($k = 1, \ldots, N$).

In [10], underwater robots with limited communication employ a leader–follower scheme for cooperative transportation, where the leader applies impedance control to follow the trajectory. Collaborative quadrotors in [11] achieve coordination without external position tracking or inter-robot communication using an adaptive ascent controller. The method of [12] is further extended in [13], [14] to teams of mobile manipulators, where impedance filters regulate both environmental and internal wrenches. Gradient projection is adopted in [15] to minimize internal wrenches on the manipulated object.

In [16], a consensus-based observer is used to estimate the complete system state, which local controllers then exploit to compute inputs for mobile manipulators. A subsequent work [17] introduces a two-stage strategy: first, an estimation of the parameters of an arbitrary object is performed; second, distributed impedance control is applied to regulate the robots. In [18], convergence of both object pose and interaction wrenches is ensured through a decentralized fuzzy control scheme that integrates disturbance observers with parameter adaptation.

In this work, we propose a two-stage decentralized admittance control framework for cooperative manipulation with N manipulators. The method regulates internal wrenches while distributing external ones across the team. The overall architecture is illustrated in Fig. 1. A round-robin communication protocol is employed, where each robot uses a momentum-based observer [19] to measure its own wrench and estimates those of its teammates. These estimates are then used to compute two compliant trajectories: one for the task object and another for the robot's motion relative to its peers, thereby reducing stress on the manipulated object.

[1] Department of Health Sciences, University of Basilicata, 85100 Potenza, Italy. {graziano.carriero, fabrizio.caccavale}@unibas.it
[2] Department of Engineering, University of Basilicata, 85100 Potenza, Italy. {monica.sileo, francesco.pierri}@unibas.it
[3]Department of Automatic Control, Lund University, 221 00 Lund, Sweden. The authors are members of the ELLIIT Strategic Research Area at Lund University. {sebastiano.fregnan, yiannis.karayiannidis}@control.lth.se
Corresponding author: Graziano Carriero.

This research was funded by the Next Generation EU-Italian National Recovery and Resilience Plan (NRRP), Mission 4, Component 1, under the program PRIN 2022 PNRR of the Italian Ministry of University and Research. Project MELODY (Multi robot collaborativE manipuLation suppOrting DisassemblY tasks) CUP C53D23008320001.

The approach is experimentally validated on a setup of three Franka Emika Panda manipulators cooperatively transporting a grasped wooden board.

II. Multi–robot system and communication topology

Consider a system composed of N manipulators cooperatively grasping a rigid object. In the absence of a central unit for information exchange, communication among the robots is modeled by a *strongly connected* directed graph $\mathcal{G}(\mathcal{R}, \mathcal{E})$, with $\mathcal{E} \subseteq \mathcal{R} \times \mathcal{R}$, where any two distinct nodes $n_i, n_j \in \mathcal{R}$ are connected by a directed path. The neighbor set of the i-th robot, containing all robots that can transmit information to it, is defined as $\mathcal{N}_i = \{j \in \mathcal{R} : (j,i) \in \mathcal{E}\}$.

The graph topology is described by the $(N \times N)$ adjacency matrix

$$\boldsymbol{A} = \{a_{ij}\} : \quad a_{ii} = 0, \quad a_{ij} = \begin{cases} 1 & \text{if } (j,i) \in \mathcal{E} \\ 0 & \text{otherwise,} \end{cases} \tag{1}$$

where $a_{ij} \neq 0$ if the j-th robot can send information to the i-th, i.e., if $j \in \mathcal{N}_i$. The corresponding $(N \times N)$ Laplacian matrix is defined as

$$\boldsymbol{L} = \{l_{ij}\} : \quad l_{ii} = \sum_{j=1, j\neq i}^{N} a_{ij}, \quad l_{ij} = -a_{ij}, \; i \neq j\,. \tag{2}$$

Each robot is assumed to know only its neighbors, without information about the full communication graph. As shown in [20], the opposite of the matrix $\bar{\boldsymbol{L}}_i$, obtained from $\boldsymbol{L}$ by removing the i-th row and column, is Hurwitz.

III. Object dynamics

Let $\boldsymbol{h}_{env}$ denote the vector of wrenches (or *generalized forces*) exerted by the object on the environment, and $\boldsymbol{h}_o$ the wrenches applied by the manipulators on the object. The object dynamics can then be expressed as

$$\boldsymbol{M}_o(\boldsymbol{x}_o)\ddot{\boldsymbol{x}}_o + \boldsymbol{C}_o(\boldsymbol{x}_o, \dot{\boldsymbol{x}}_o)\dot{\boldsymbol{x}}_o + \boldsymbol{g}_o = \boldsymbol{\gamma}_o - \boldsymbol{\gamma}_{env}\,, \tag{3}$$

where $\boldsymbol{x}_o = [\boldsymbol{p}_o^{\mathrm{T}} \; \boldsymbol{\phi}_o^{\mathrm{T}}]^{\mathrm{T}}$ $(\dot{\boldsymbol{x}}_o, \ddot{\boldsymbol{x}}_o)$ is the object pose (generalized velocity, generalized acceleration), with $\boldsymbol{p}_o$ and $\boldsymbol{\phi}_o$ denoting position and Euler-angle orientation. Here, $\boldsymbol{M}_o$ is the inertia matrix, $\boldsymbol{C}_o$ the Coriolis/centripetal matrix, and $\boldsymbol{g}_o$ the gravity term. The wrenches are mapped as

$$\boldsymbol{\gamma}_{env} = \boldsymbol{T}_A^{\mathrm{T}}(\boldsymbol{\phi}_o)\boldsymbol{h}_{env}, \quad \boldsymbol{\gamma}_o = \boldsymbol{T}_A^{\mathrm{T}}(\boldsymbol{\phi}_o)\boldsymbol{h}_o,$$

via the matrix

$$\boldsymbol{T}_A(\boldsymbol{\phi}_o) = \begin{bmatrix} \boldsymbol{I}_3 & \boldsymbol{O}_3 \\ \boldsymbol{O}_3 & \boldsymbol{T}(\boldsymbol{\phi}_o) \end{bmatrix},$$

where $\boldsymbol{T}(\boldsymbol{\phi}_o)$ relates the Euler angle rates $\dot{\boldsymbol{\phi}}_o$ to the angular velocity $\boldsymbol{\omega}_o$ [21], and $\boldsymbol{I}_n$, $\boldsymbol{O}_n$ denote the $(n \times n)$ identity and null matrices, respectively.

The wrench $\boldsymbol{h}_o$ is computed through the *grasp matrix* $\boldsymbol{G}$ [12]:

$$\boldsymbol{h}_o = \begin{bmatrix} \boldsymbol{I}_3 & \boldsymbol{O}_3 & \dots & \boldsymbol{I}_3 & \boldsymbol{O}_3 \\ \boldsymbol{S}(\boldsymbol{r}_1) & \boldsymbol{I}_3 & \dots & \boldsymbol{S}(\boldsymbol{r}_N) & \boldsymbol{I}_3 \end{bmatrix} \begin{bmatrix} \boldsymbol{h}_1 \\ \vdots \\ \boldsymbol{h}_N \end{bmatrix} = \boldsymbol{G}\boldsymbol{h}_e, \tag{4}$$

with

$$\boldsymbol{G} = \begin{bmatrix} \boldsymbol{G}_1 & \boldsymbol{G}_2 & \dots & \boldsymbol{G}_N \end{bmatrix}, \quad \boldsymbol{G}_k = \begin{bmatrix} \boldsymbol{I}_3 & \boldsymbol{O}_3 \\ \boldsymbol{S}(\boldsymbol{r}_k) & \boldsymbol{I}_3 \end{bmatrix}, \tag{5}$$

where $\boldsymbol{S}(\cdot)$ is the skew-symmetric operator, $\boldsymbol{r}_k = \boldsymbol{p}_k - \boldsymbol{p}_o$ is the vector from the object origin to the k-th end-effector (often referred as *virtual stick*) [22]. Thus, $\boldsymbol{h}_o$ represents the wrenches at the object center of mass, denominated as *external wrenches*, while $\boldsymbol{h}_e = [\boldsymbol{h}_1^{\mathrm{T}} \; \dots \; \boldsymbol{h}_N^{\mathrm{T}}]^{\mathrm{T}}$ collects the wrenches applied by each end effector.

Since $\boldsymbol{G}$ has full row rank, (4) admits the inverse solution [23]:

$$\boldsymbol{h} = \boldsymbol{G}^{\dagger}\boldsymbol{h}_o + \boldsymbol{V}\boldsymbol{h}_i = \boldsymbol{h}_E + \boldsymbol{h}_I, \tag{6}$$

where $\boldsymbol{G}^{\dagger}$ is a right pseudo-inverse of $\boldsymbol{G}$, $\boldsymbol{V} \in \mathbb{R}^{6N \times (6N-6)}$ is a full-column rank matrix which spans the null space of $\boldsymbol{G}$, and $\boldsymbol{h}_i \in \mathbb{R}^{6N-6}$ collects the independent wrenches that do not affect object motion, i.e., the *internal wrenches* [22]. These arise when manipulator forces lie in the null space of the grasp matrix and result from trajectory-tracking uncertainties or physical constraints. Although they do not affect object motion, they may induce undesired stresses and should be minimized.

Following [23], we adopt the basis

$$\boldsymbol{V} = \begin{bmatrix} -\boldsymbol{V}_1 & \boldsymbol{O}_6 & \dots & \boldsymbol{O}_6 \\ \boldsymbol{O}_6 & -\boldsymbol{V}_2 & \dots & \boldsymbol{O}_6 \\ \vdots & \vdots & \ddots & \vdots \\ \boldsymbol{O}_6 & \boldsymbol{O}_6 & \dots & -\boldsymbol{V}_{N-1} \\ \boldsymbol{V}_N & \boldsymbol{V}_N & \dots & \boldsymbol{V}_N \end{bmatrix}, \boldsymbol{V}_k = \begin{bmatrix} \boldsymbol{I}_3 & \boldsymbol{O}_3 \\ -\boldsymbol{S}(\boldsymbol{r}_k) & \boldsymbol{I}_3 \end{bmatrix}. \tag{7}$$

Accordingly, $\boldsymbol{h}_E$ denotes the external contribution balancing the object dynamics and the interaction with the environment,

$$\boldsymbol{h}_E = \begin{bmatrix} \boldsymbol{h}_{E_1}^{\mathrm{T}} & \dots & \boldsymbol{h}_{E_N}^{\mathrm{T}} \end{bmatrix}^{\mathrm{T}} = \boldsymbol{G}^{\dagger}\boldsymbol{G}\boldsymbol{h}_e, \tag{8}$$

while $\boldsymbol{h}_I$ captures the robots' contribution to the internal wrench:

$$\boldsymbol{h}_I = \begin{bmatrix} \boldsymbol{h}_{I_1}^{\mathrm{T}} & \dots & \boldsymbol{h}_{I_N}^{\mathrm{T}} \end{bmatrix}^{\mathrm{T}} = \boldsymbol{V}\boldsymbol{h}_i = \boldsymbol{V}\boldsymbol{V}^{\dagger}\boldsymbol{h}_e. \tag{9}$$

A. Closed-Chain Constraints

Let us consider the planning of an object trajectory in terms of position, $\boldsymbol{p}_{o,d}$, and orientation, $\boldsymbol{\phi}_{o,d}$ (expressed, e.g., using Euler angles). By enforcing the closed-chain constraints of the system composed of the object and the N manipulators, the desired motion of each end-effector, $\boldsymbol{x}_{k,d} = \begin{bmatrix} \boldsymbol{p}_{k,d}^{\mathrm{T}}, \boldsymbol{\phi}_{k,d}^{\mathrm{T}} \end{bmatrix}^{\mathrm{T}}$, can be derived according to the following relations [12]:

$$
\begin{cases}
\boldsymbol{p}_{k,d} = & \boldsymbol{p}_{o,d} + \boldsymbol{r}_{k,d} \\
\dot{\boldsymbol{p}}_{k,d} = & \dot{\boldsymbol{p}}_{o,d} - \boldsymbol{S}(\boldsymbol{r}_{k,d})\boldsymbol{T}(\boldsymbol{\phi}_{o,d})\dot{\boldsymbol{\phi}}_{o,d} \\
\ddot{\boldsymbol{p}}_{k,d} = & \ddot{\boldsymbol{p}}_{o,d} - \boldsymbol{S}(\boldsymbol{r}_{k,d})\dot{\boldsymbol{T}}(\boldsymbol{\phi}_{o,d})\dot{\boldsymbol{\phi}}_{o,d} + \\
& -\boldsymbol{S}(\boldsymbol{T}(\boldsymbol{\phi}_{o,d})\dot{\boldsymbol{\phi}}_{o,d})\boldsymbol{S}(\boldsymbol{r}_{k,d})\boldsymbol{T}(\boldsymbol{\phi}_{o,d})\dot{\boldsymbol{\phi}}_{o,d} + \\
& -\boldsymbol{S}(\boldsymbol{r}_{k,d})\boldsymbol{T}(\boldsymbol{\phi}_{o,d})\ddot{\boldsymbol{\phi}}_{o,d} \\
\boldsymbol{\phi}_{k,d} = & \boldsymbol{\phi}(\boldsymbol{R}_{o,d}\boldsymbol{R}^{o}_{k,d}) \\
\dot{\boldsymbol{\phi}}_{k,d} = & \boldsymbol{T}^{-1}(\boldsymbol{\phi}_{k,d})\boldsymbol{T}(\boldsymbol{\phi}_{o,d})\dot{\boldsymbol{\phi}}_{o,d} \\
\ddot{\boldsymbol{\phi}}_{k,d} = & \boldsymbol{T}^{-1}(\boldsymbol{\phi}_{k,d})\dot{\boldsymbol{T}}(\boldsymbol{\phi}_{o,d})\dot{\boldsymbol{\phi}}_{o,d} + \\
& \boldsymbol{T}^{-1}(\boldsymbol{\phi}_{k,d})(\boldsymbol{T}(\boldsymbol{\phi}_{o,d})\ddot{\boldsymbol{\phi}}_{o,d} - \dot{\boldsymbol{T}}(\boldsymbol{\phi}_{k,d})\dot{\boldsymbol{\phi}}_{k,d})
\end{cases}
\tag{10}
$$

where $\boldsymbol{\phi}(\boldsymbol{R})$ denotes the set of Euler angles extracted from the rotation matrix $\boldsymbol{R}$, while $\boldsymbol{R}_{o,d}$ and $\boldsymbol{R}^{o}_{k,d}$ represent, respectively, the desired orientation of the object and the desired orientation of the k-th end-effector expressed in the object reference frame Σ_o.

IV. Decentralized wrench estimation

In view of (4) and (9), the computation of internal and external wrenches requires knowledge of each robot's contribution exerted at its own end-effector, $\boldsymbol{h}_e$. This, in turn, implies either the existence of a centralized unit that collects all generalized forces and computes the manipulators' control laws, or an all-to-all communication scheme among the robots. Both solutions, however, pose limitations in terms of scalability and robustness, as they entail an increasing computational burden with the team size.

An alternative strategy consists in interpreting each robot as the *leader* of its own wrench signal, with the remaining robots acting as *followers*. Unlike the method proposed in [24], this approach requires the communication graph among the robots to be strongly connected. In this framework, each agent estimates the wrenches exerted by the other $N-1$ robots by running a bank of $N-1$ consensus-based estimators, defined as

$$
{}^{i}\dot{\hat{\boldsymbol{h}}}_k(t) = k_0 \sum_{j \in \mathcal{N}_i} \left({}^{j}\hat{\boldsymbol{h}}_k(t) - {}^{i}\hat{\boldsymbol{h}}_k(t) \right), \tag{11}
$$

where ${}^{i}\dot{\hat{\boldsymbol{h}}}_k(t)$ denotes the estimate, computed by the i-th manipulator, of the wrench exerted on the object by the k-th manipulator ($k = 1, \dots, N$), and k_0 is a positive scalar gain.

Then, the dynamics of the estimation error, ${}^{i}\widetilde{\boldsymbol{h}}_k$, can be derived straightforwardly:

$$
\begin{aligned}
{}^{i}\dot{\widetilde{\boldsymbol{h}}}_k &= \dot{\boldsymbol{h}}_k - {}^{i}\dot{\hat{\boldsymbol{h}}}_k = \dot{\boldsymbol{h}}_k - k_0 \sum_{j \in \mathcal{N}_i} \left({}^{i}\widetilde{\boldsymbol{h}}_k - {}^{j}\widetilde{\boldsymbol{h}}_k \right) \\
&= \dot{\boldsymbol{h}}_k - k_0 N_i {}^{i}\widetilde{\boldsymbol{h}}_k + k_0 \sum_{j \in \mathcal{N}_i} {}^{j}\widetilde{\boldsymbol{h}}_k,
\end{aligned} \tag{12}
$$

where N_i is the cardinality of the set of neighbors of the i-th robot. Let's define the $6(N-1) \times 1$ vector, $\hat{\boldsymbol{h}}_k$, which collects the estimates of $\boldsymbol{h}_k$ provided by each robot but the k-th and the corresponding collective estimation error, $\widetilde{\boldsymbol{h}}_k$, as

$$
\begin{aligned}
\hat{\boldsymbol{h}}_k &= \begin{bmatrix} {}^{1}\hat{\boldsymbol{h}}_k^{\mathrm{T}} & \dots & {}^{k-1}\hat{\boldsymbol{h}}_k^{\mathrm{T}} & {}^{k+1}\hat{\boldsymbol{h}}_k^{\mathrm{T}} & \dots & {}^{N}\hat{\boldsymbol{h}}_k^{\mathrm{T}} \end{bmatrix}^{\mathrm{T}}, \\
\widetilde{\boldsymbol{h}}_k &= (\boldsymbol{1}_{N-1} \otimes \boldsymbol{h}_k) - \hat{\boldsymbol{h}}_k,
\end{aligned} \tag{13}
$$

where $\otimes$ denotes the Kronecker product [25]. The collective error dynamics $\dot{\widetilde{\boldsymbol{h}}}_k$ is given by

$$
\dot{\widetilde{\boldsymbol{h}}}_k = (\boldsymbol{1}_{N-1} \otimes \dot{\boldsymbol{h}}_k) + \bar{\boldsymbol{L}}_0 \widetilde{\boldsymbol{h}}_k, \tag{14}
$$

where $\bar{\boldsymbol{L}}_0 = (-\bar{\boldsymbol{L}} \otimes \boldsymbol{I}_6)$. By exploiting the results in [26], the $-\bar{\boldsymbol{L}}$ matrix is Hurwitz and, consequently, due to the Kroneker product properties, $\bar{\boldsymbol{L}}_0$ is Hurwitz as well. Therefore, it is straightforward to prove that $\widetilde{\boldsymbol{h}}_k$ is asymptotically convergent to zero in the presence of constant or slowly variant wrenches $\boldsymbol{h}_k$, while it is bounded in the presence of a bounded time derivative $\dot{\boldsymbol{h}}_k$.

Let's define as ${}^{i}\hat{\boldsymbol{h}}_e$ the i-th robot estimate of the end-effector wrench collective vector

$$
{}^{i}\hat{\boldsymbol{h}}_e = \begin{bmatrix} {}^{i}\hat{\boldsymbol{h}}_1^{\mathrm{T}} & \dots & {}^{i}\hat{\boldsymbol{h}}_{i-1}^{\mathrm{T}} & \boldsymbol{h}_i^{\mathrm{T}} & {}^{i}\hat{\boldsymbol{h}}_{i+1}^{\mathrm{T}} & \dots & {}^{i}\hat{\boldsymbol{h}}_N^{\mathrm{T}} \end{bmatrix}^{\mathrm{T}}. \tag{15}
$$

Firstly, the i-th robot can reduce its estimate of the external wrenches exerted on the object ${}^{i}\hat{\boldsymbol{h}}_o$ by resorting to (4):

$$
{}^{i}\hat{\boldsymbol{h}}_o = \boldsymbol{G}\, {}^{i}\hat{\boldsymbol{h}}_e \tag{16}
$$

Secondly, it can limit its own contribution to the internal wrench defined in (9) as

$$
{}^{i}\hat{\boldsymbol{h}}_{I_i} = \boldsymbol{\Gamma}_i \boldsymbol{V} \boldsymbol{V}^{\dagger}\, {}^{i}\hat{\boldsymbol{h}}_e, \tag{17}
$$

where $\boldsymbol{\Gamma}_i = \{\boldsymbol{O}_6 \quad \cdots \quad \underbrace{\boldsymbol{I}_6}_{i\text{-th robot}} \quad \cdots \quad \boldsymbol{O}_6\} \in \mathbb{R}^{6 \times 6N}$.

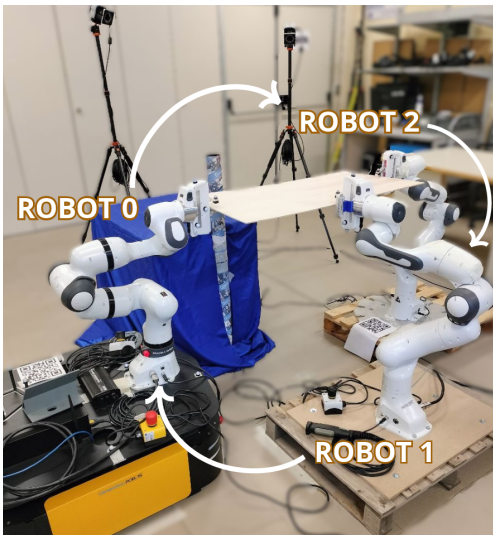

Fig. 2. The experimental setup: the piece is grasped and transported by the robots. The base frame of the robot mounted on the mobile base is set as the world frame Σ_w. A cylindrical obstacle is placed within the robot team's workspace, firmly fixed to a heavy support. The communication graph consists of 3 nodes arranged in a cycle graph.

V. Decentralized admittance control

The proposed strategy relies on a two-stage admittance-based framework designed to minimize the internal stresses acting on the manipulated object, while ensuring bounded contact forces with the environment in a fully decentralized manner. The control architecture of the i-th robot ($i = 1, \dots, N$) is organized into the following hierarchical levels:

- the *outer loop* (external impedance loop) computes the object reference trajectory, $\boldsymbol{x}_{o_r},\ \dot{\boldsymbol{x}}_{o_r},\ \ddot{\boldsymbol{x}}_{o_r}$, while distributing the external wrench applied to the object;
- the *inner loop* (internal impedance loop) generates the end-effector reference trajectory of the i-th robot, $\boldsymbol{x}_{i_r},\ \dot{\boldsymbol{x}}_{i_r},\ \ddot{\boldsymbol{x}}_{i_r}$, while limiting its contribution to the internal wrenches;
- finally, a motion controller is employed to track the reference trajectory; in principle, any suitable low-level motion control strategy can be adopted.

A key feature of this framework lies in its flexibility: external and internal motion variables are decoupled, allowing the activation or deactivation of each impedance filter independently or in combination, without compromising the overall control performance.

The desired object trajectory is provided to the external impedance filter together with the estimates of the external wrenches obtained from (16). The object reference motion variables are then computed by integrating the following differential equation:

$$(\boldsymbol{A} - \boldsymbol{I}_6)\boldsymbol{M}_o\ddot{\boldsymbol{x}}_{o_r} + \boldsymbol{D}_o\dot{\boldsymbol{x}}_{o_r} + \boldsymbol{K}_o\boldsymbol{x}_{o_r} + {}^i\hat{\boldsymbol{\gamma}}_o = \boldsymbol{C}_o\dot{\boldsymbol{x}}_o + \boldsymbol{g}_o + \boldsymbol{A}\boldsymbol{M}_o\ddot{\boldsymbol{x}}_{o_d} + \boldsymbol{D}_o\ddot{\boldsymbol{x}}_{o_d} + \boldsymbol{K}_o\boldsymbol{x}_{o_d}, \quad (18)$$

whose asymptotic stability is ensured provided that the eigenvalues of the positive definite diagonal matrix $\boldsymbol{A}$ are greater than or equal to 1.

Assume that the low-level tracking is perfect, i.e., the actual and reference poses of the object coincide, $\boldsymbol{x}_o = \boldsymbol{x}_{o_r}$. This assumption is reasonable, given the slow trajectories typically adopted in cooperative transportation tasks. By substituting the object dynamics into the differential equation, the desired object behavior is expressed as

$$\boldsymbol{A}\boldsymbol{M}_o\ddot{\boldsymbol{e}}_o + \boldsymbol{D}_o\dot{\boldsymbol{e}}_o + \boldsymbol{K}_o\boldsymbol{e}_o = {}^i\hat{\boldsymbol{\gamma}}_{env}, \quad (19)$$

where $\boldsymbol{e}_o = \boldsymbol{x}_{o_d} - \boldsymbol{x}_o$. Thus, the object behavior can be shaped by properly tuning the positive definite matrices representing inertia ($\boldsymbol{A}\boldsymbol{M}_o$), damping ($\boldsymbol{D}_o$), and stiffness ($\boldsymbol{K}_o$). The output of the external impedance filter is then mapped to the end-effector motion variables through the closed-chain constraints (10), and subsequently fed into the internal impedance filter. The latter processes both local kinematic and dynamic inputs: the i-th end-effector desired trajectory and the i-th robot contribution to the internal wrench, obtained from (17). Noticeably, this filter does not alter the object trajectory; instead, it regulates the i-th end-effector reference motion to prevent excessive internal forces and moments, according to

$$\ddot{\boldsymbol{x}}_{r_i} = \ddot{\boldsymbol{x}}_{d_i} + \boldsymbol{M}_i^{-1}\left[\boldsymbol{D}_i(\dot{\boldsymbol{x}}_{d_i} - \dot{\boldsymbol{x}}_{r_i}) + \boldsymbol{K}_i(\boldsymbol{x}_{d_i} - \boldsymbol{x}_{r_i}) + {}^i\hat{\boldsymbol{h}}_{I_i}\right] \quad (20)$$

where $\boldsymbol{D}_i$, $\boldsymbol{K}_i$, and $\boldsymbol{M}_i$ are (6×6) positive definite gain matrices that define, respectively, virtual damping, stiffness, and inertia for the i-th end-effector motion.

VI. Experimental results

Consider a cooperative robotic cell composed of $N = 3$ Franka Emika Panda arms. One manipulator is mounted on a mobile base, which is mechanically braked for the purposes of this study. The multi-robot system executes a cooperative object transportation task in a fully decentralized manner. Each agent is assumed to be provided *a priori* with the desired object trajectory, i.e., positions, orientations, and their time derivatives, which serve as input to the external admittance controller (Section V). A detailed description of the experimental setup is reported in Appendix I.

A dedicated ROS node is assigned to each robot, enabling communication and data exchange according to the topology shown in Fig. 2.

The decentralized scheme consists of three steps: (i) a *wrench estimation* phase, (ii) the external admittance filter, and (iii) the internal admittance filter (see Section V).

At each time instant, the i-th robot acquires the wrench estimated by its momentum-based observer, $\boldsymbol{h}_i$, together with the wrench estimates from its neighbors, ${}^i\hat{\boldsymbol{h}}_{j\neq i}$. To account for communication delays and packet losses, these signals are synchronized using the ROS *TimeSynchronizer* filter. Then, based on (11), the i-th robot reconstructs the collective end-effector wrench vector, ${}^i\hat{\boldsymbol{h}}_e$, and publishes it on a dedicated ROS topic. From this information, the external generalized forces acting on the object center of mass are computed via (16), together with the i-th robot's contribution to the internal wrench via (17).

The estimated external wrenches are subsequently processed by the external admittance filter (18), together with the desired object trajectory. As a result, each robot computes the object reference trajectory in terms of position, velocity, and acceleration. This reference is then mapped through the closed-chain constraints, yielding the i-th end-effector trajectory. Finally, this trajectory, along with the i-th robot's internal wrench contribution, is fed into the local internal admittance filter (20), whose output is published on a specific ROS topic to be subscribed by the robot's low-level controller node.

The task under consideration consists of the decentralized cooperative transportation of a rectangular wooden piece of dimensions $90 \times 45 \times 0.6$ cm and mass $m_o = 0.8$ kg, performed by 3 manipulators as illustrated in Fig. 2.

Let us introduce an inertial frame Σ_w, coincident with the base frame Σ_0 of the manipulator mounted on the mobile base (hereafter referred to as Robot 0). The desired trajectory of the object barycenter is designed to assess the applicability of the proposed strategy and consists of a translation along an arc of circumference with radius $r = 0.3$ m and angle $\theta_p = \pi/8$ rad, combined with a rotation about the z-axis of $\theta_o = \pi/8$ rad. The task is scheduled to be completed in 20 s: it begins with an initial steady-state phase of 2 s, followed by 15 s of motion, and ends with 3 s of steady state. At the

initial time instant, the robotic team is already cooperatively grasping the object. During the execution, the object moves freely without environmental interactions until approximately $t = 11$ s, when it collides with a curved surface.

Since the admittance law (20) is formulated with respect to the world frame Σ_w, the reference trajectories sent to Robots 1 and 2 must be transformed into their respective base frames, Σ_1 and Σ_2. This transformation is achieved through the homogeneous matrices $\boldsymbol{T}_1^w$ and $\boldsymbol{T}_2^w$, which encode the pose of each robot base frame relative to Σ_w. The matrices $\boldsymbol{T}_1^w$ and $\boldsymbol{T}_2^w$ are obtained via a calibration procedure performed with a Vicon motion capture system. More in detail, six infrared cameras are adopted to measure the pose of each robot end-effector with respect to the Vicon base frame. By exploiting the robots' inverse kinematics, the relative poses of their base frames with respect to Σ_w can then be straightforwardly determined.

Four experiments were conducted to evaluate the effectiveness of the estimator–controller architecture presented in Section V. In the first case study, the robots cooperatively grasping the object were regulated solely through the baseline low-level positional controller. In the second and third experiments, the external and the internal admittance filters were independently activated, thereby isolating their individual contributions. Finally, the fourth experiment employed the full proposed controller with both the external and internal admittance filters, demonstrating the complete capabilities of the proposed approach.

The gains in (18) and (20) have been set to:

- $\boldsymbol{A} = \mathrm{diag}\{10,\ 10,\ 15,\ 10,\ 10,\ 10\}$,
  $\boldsymbol{K}_o = \mathrm{diag}\{15,\ 15,\ 25,\ 7.5,\ 7.5,\ 7.5\}$,
  $\boldsymbol{D}_o = \mathrm{diag}\{75,\ 75,\ 75,\ 50,\ 50,\ 50\}$,

and

- $\boldsymbol{M}_i = \mathrm{diag}\{15,\ 15,\ 15,\ 5,\ 5,\ 5\}$,
  $\boldsymbol{K}_i = \mathrm{diag}\{45,\ 45,\ 50,\ 15,\ 15,\ 15\}$,
  $\boldsymbol{D}_i = \mathrm{diag}\{80,\ 80,\ 80,\ 25,\ 25,\ 25\}$.

For both the object and the robots, the damping gains $\boldsymbol{D}_o$ and $\boldsymbol{D}_i$ were tuned to guarantee a well-damped response, while the stiffness matrices $\boldsymbol{K}_o$ and $\boldsymbol{K}_i$ were selected to ensure a compliant behavior.

A dead-zone on both the admittance filter inputs has been applied in order to eliminate sensor noise and non-perfect gravity compensations.

Figure 3 shows the end-effector wrench estimation errors ${}^i\widetilde{\boldsymbol{h}}_k$ for each agent, normalized with respect to the norm of the corresponding measured wrenches $\boldsymbol{h}_k$. For compactness, only the results of the first case study are reported, as they are representative of the other cases as well. Remarkably, even in the absence of any admittance controller, the impact between the object and the obstacle—producing an impulsive increase in the applied wrench—does not compromise the estimation performance: errors remain bounded throughout the experiment and reach their maximum absolute value at the instant of collision, remaining $\leq 5\%$.

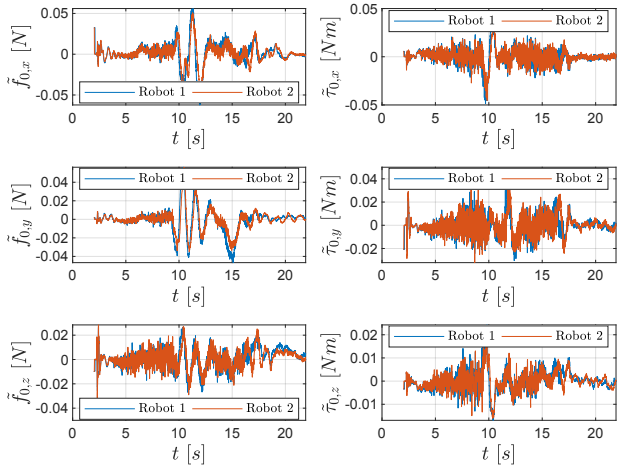

(a) Estimation error $\widetilde{\boldsymbol{h}}_0$ provided by Robot 1 and Robot 2.

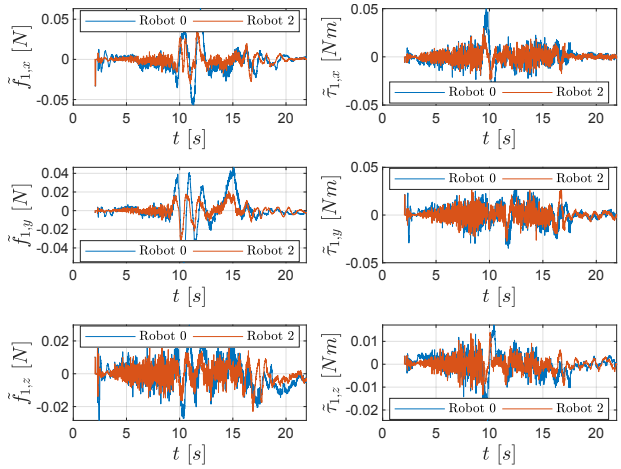

(b) Estimation error $\widetilde{\boldsymbol{h}}_1$ provided by Robot 0 and Robot 2.

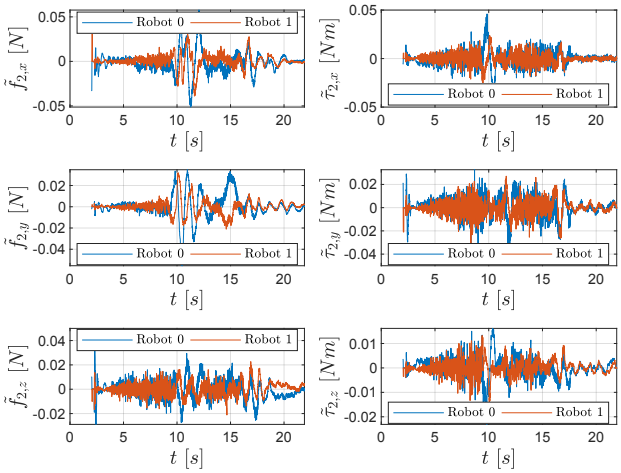

(c) Estimation error $\widetilde{\boldsymbol{h}}_2$ provided by Robot 0 and Robot 1.

Fig. 3. Wrench estimation errors $\widetilde{\boldsymbol{h}}_k$.

A. Positional Controller

In the first use case, no impedance filter is activated, and the robots directly track the desired trajectory derived from the closed-chain constraints in (10), neglecting any force feedback. As shown in Fig. 4, at the initial time instant the robots experience a positive external torque along the z-axis, which is almost completely nullified upon contact

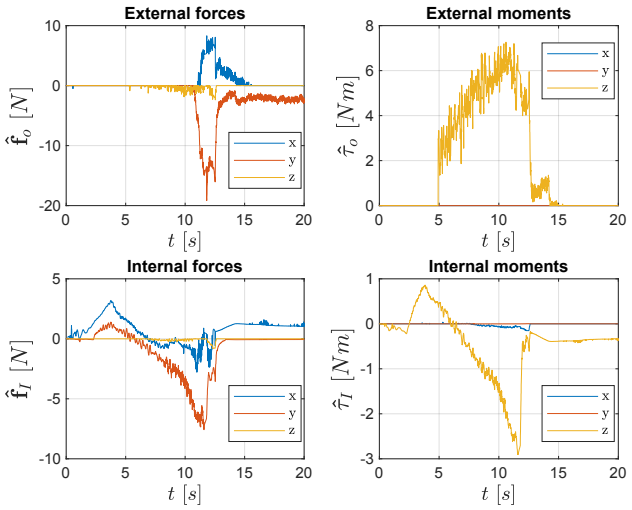

Fig. 4. *Positional controller* case study: external wrenches (top) and internal wrenches (bottom).

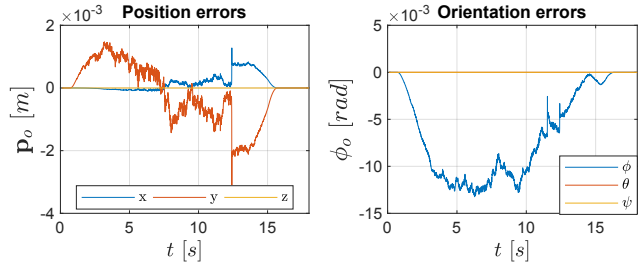

Fig. 5. *Positional controller* case study: position errors (left) and orientation errors (right).

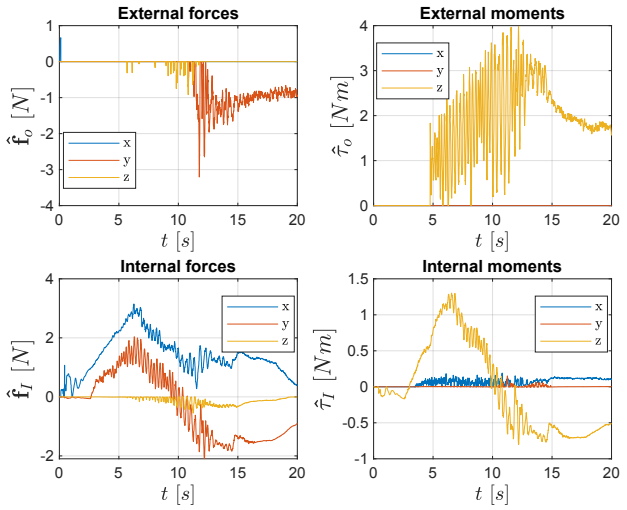

Fig. 6. *External admittance controller* case study: external wrenches (top) and internal wrenches (bottom).

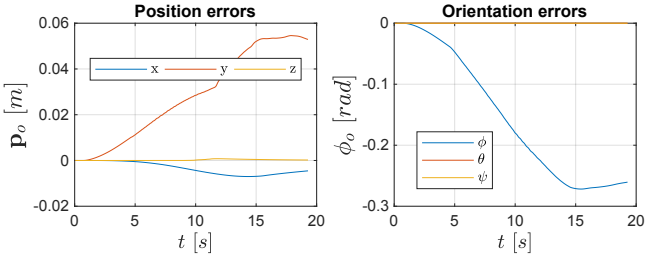

Fig. 7. *External admittance controller* case study: position errors (left) and orientation errors (right).

with the obstacle. This effect arises because the rotational motion around the z-axis terminates at impact, leading to a near cancellation of torques, with only a small residual sliding along the curved contact surface. The geometry of this surface allows the object to slightly continue its rotational motion around the vertical axis.

At the same time, the collision induces an increase in the external forces within the x–y plane, as expected. In particular, two peaks in the external force along the y-axis are observed. These peaks can be attributed to slipping of the object between the fingertips of one of the robots, positioned opposite the obstacle with respect to the object's barycenter. This is followed by a phase in which the external forces remain constant. Consequently, the internal force along the y-axis decreases significantly, leading to a relaxation of both the internal force and the internal torque squeezing the object.

Fig. 5 reports the time histories of the object's position and orientation errors. Upon contact with the obstacle, the position error exhibits an instantaneous increase before subsequently decreasing. In contrast, the curved contact surface mitigates variations in the orientation error, allowing it to remain consistently low throughout the interaction.

B. External admittance

The adoption of the external admittance filter considerably reduces the external torques applied to the object during the rotational phase preceding the contact with the obstacle (Fig. 6). After contact, the external torque signal becomes smoother and settles at a constant value during the final steady-state phase. A similar behavior is observed in the external forces: along the x-axis, they remain within the dead-zone, whereas along the y-axis an impulsive increase occurs due to the collision, followed by stabilization at a constant value. Compared to the positional control case, the external forces after the collision are significantly reduced.

As expected, internal forces and torques do not exhibit substantial deviations from those observed in the pure positional control scenario. However, after contact, their absolute values remain lower, and no impulsive drop associated with the object slipping through the robot grippers is observed. Consequently, both internal forces and torques remain nearly constant until the end of the experiment.

The reduction of the external wrenches results, as expected, in larger position errors-mainly along the y-axis, which experiences the highest external force-and orientation errors around the z-axis (Fig. 7). These error values remain approximately constant during the final steady-state phase.

C. Internal admittance

Activating the internal admittance filter significantly reduces internal forces and torques, as shown in Fig. 8. Before the contact with the obstacle, both the internal forces in the horizontal plane and the internal torques around the vertical axis do not exhibit the increasing trend observed in the

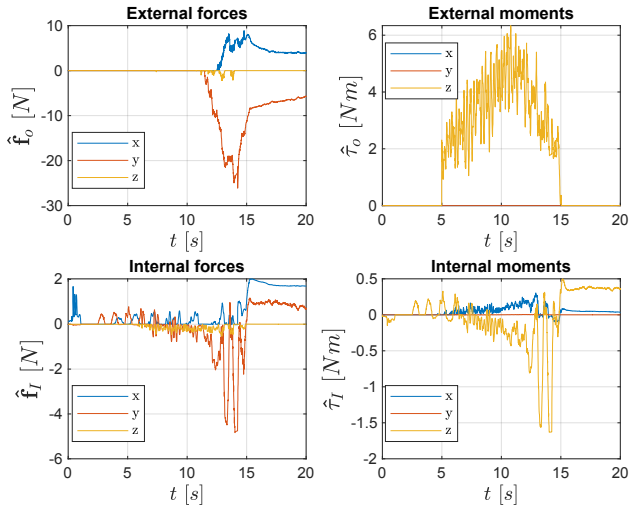

Fig. 8. *Internal admittance controller* case study: external wrenches (top) and internal wrenches (bottom).

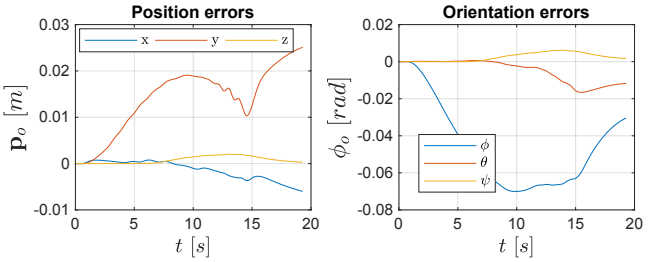

Fig. 9. *Internal admittance controller* case study: position errors (left) and orientation errors (right).

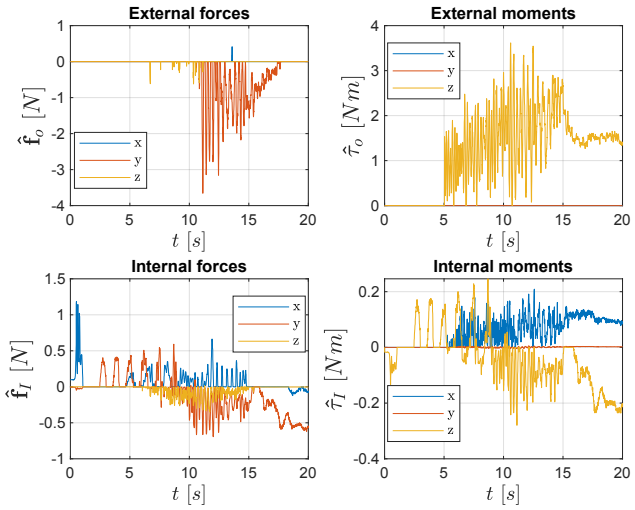

Fig. 10. *External and internal admittance controller* case study: external wrenches (top) and internal wrenches (bottom).

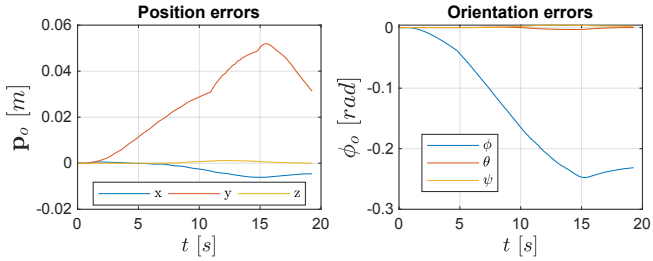

Fig. 11. *External and internal admittance controller* case study: position errors (left) and orientation errors (right).

previous case studies, but instead remain bounded. Due to the absence of the external admittance, however, the collision leads to peaks in the internal force along the y-axis and the internal torque around the z-axis, caused by slight slipping of the object between the robot grippers.

A slight coupling between internal and external torques can be noticed when analyzing the external force along the z-axis and the object errors (Fig. 9): no force values leave the dead-zone, unlike in the previous two cases, where such deviations are likely due to deformations of the object caused by higher internal forces and torques. Moreover, the external forces remain constant, since, although the position and orientation errors are clearly lower than in the external admittance case, they are still higher than in the positional control case. As a result, the object pushes against the environment surface, leading to high forces and torques.

D. External and internal admittance

In the last case study, both the external and the internal admittance are activated. As a consequence, the external wrenches exhibit a behavior nearly identical to that of the second case study (external admittance only), as do the position and orientation errors, confirming the decoupling between the two filters (Figs. 10 and 11). Since no actual collision with the environment occurs, and consequently no slipping of the object takes place, internal forces and torques remain bounded and very low in absolute value throughout the entire experiment.

The object's flexibility leads to the presence of external torques along the z-axis and external forces along the x- and y-axes. A slight misalignment of the robots with respect to the vertical axis causes the appearance of an internal torque around the x-axis.

This paper presents a decentralized strategy for cooperative object transportation with multiple manipulators, based on a two-loop admittance control scheme. The approach guarantees bounded external and internal wrenches, with coordination achieved through a round-robin communication scheme.

VII. Conclusions and Future Works

Experiments with 3 Franka Emika Panda robots confirm a significant reduction of both external and internal wrenches when the two admittance filters are enabled.

Future work will address the stability of a fully decentralized implementation without assuming a priori knowledge of the object trajectory, and extend the validation to mobile-based manipulators.

Appendix I
Experimental Setup

Three Franka Emika Panda robots are employed in the experimental setup presented in this work. These are 7-DOF anthropomorphic manipulators, featuring rotational joints, a maximum payload capacity of 3 kg, and a repeatability of 0.1 mm. Each robot is equipped with the integrated end-effector

Franka Hand. Robot control is implemented via the open-source package *franka_ros*, which serves as a ROS wrapper for the low-level Franka Control Interface (FCI) provided through the libfranka C++ library. The FCI offers direct access to the robot's actuators and sensors and supports real-time communication at frequencies up to 1 kHz. This enables external controllers to interact directly with the robot's internal control loop by sending commands and receiving measurements with low latency. In the proposed setup, each robot receives joint velocity commands from a Closed-Loop Inverse Kinematics (CLIK) controller [27] at every control cycle. In turn, the robot provides measured joint torques as feedback, leveraging the built-in torque sensors available at each joint, which stream data at 1 kHz via dedicated ROS nodes interfacing with the FCI. Although the Panda robot state can be updated at 1 kHz, the overall control scheme runs at a lower frequency due to synchronization requirements among the three ROS topics where the wrench signals are exchanged. Despite using the *Approximate Time* policy provided by the ROS message filters, this synchronization overhead imposes a lower effective control rate, which settles around approximately 250 Hz.

REFERENCES

[1] X. An, C. Wu, Y. Lin, M. Lin, T. Yoshinaga, and Y. Ji, "Multi-robot systems and cooperative object transport: Communications, platforms, and challenges," *IEEE Open Journal of the Computer Society*, vol. 4, pp. 23–36, 2023.

[2] F. Huzaefa and Y.-C. Liu, "Centralized control architecture for cooperative object transportation using multiple omnidirectional agvs," in *2019 IEEE/RSJ International Conference on Intelligent Robots and Systems (IROS)*. IEEE, 2019, pp. 6526–6532.

[3] H. A. Park and C. G. Lee, "Dual-arm coordinated-motion task specification and performance evaluation," in *2016 IEEE/RSJ International Conference on Intelligent Robots and Systems (IROS)*, 2016, pp. 929–936.

[4] D. Almeida and Y. Karayiannidis, "Asymmetric Dual-Arm Task Execution Using an Extended Relative Jacobian," in *Robotics Research*, T. Asfour, E. Yoshida, J. Park, H. Christensen, and O. Khatib, Eds. Cham: Springer International Publishing, 2022, vol. 20, pp. 18–34, series Title: Springer Proceedings in Advanced Robotics. [Online]. Available: https://link.springer.com/10.1007/978-3-030-95459-8_2

[5] A. Tagliabue, M. Kamel, S. Verling, R. Siegwart, and J. Nieto, "Collaborative transportation using mavs via passive force control," in *2017 IEEE International Conference on Robotics and Automation (ICRA)*. IEEE, 2017, pp. 5766–5773.

[6] A. Heins and A. P. Schoellig, "Keep it upright: Model predictive control for nonprehensile object transportation with obstacle avoidance on a mobile manipulator," *IEEE Robotics and Automation Letters*, 2023.

[7] J. Markdahl, Y. Karayiannidis, X. Hu, and D. Kragic, "Distributed cooperative object attitude manipulation," in *2012 IEEE International Conference on Robotics and Automation*. IEEE, 2012, pp. 2960–2965.

[8] N. Hogan, "Impedance control: An approach to manipulation: Parts i-iii," *J. Dyn. Sys., Meas., Control.*, vol. 107, no. 1, pp. 1–24, 1985.

[9] C. Ott, R. Mukherjee, and Y. Nakamura, "Unified impedance and admittance control," in *2010 IEEE international conference on robotics and automation*. IEEE, 2010, pp. 554–561.

[10] S. Heshmati-Alamdari, C. P. Bechlioulis, G. C. Karras, and K. J. Kyriakopoulos, "Decentralized impedance control for cooperative manipulation of multiple underwater vehicle manipulator systems under lean communication," in *2018 IEEE/OES Autonomous Underwater Vehicle Workshop (AUV)*. IEEE, 2018, pp. 1–6.

[11] M. Pokornỳ, J. Nowaková, and T. Dočekal, "Adaptive ascent control of a collaborative object transportation system using two quadrotors," *Sensors*, vol. 22, no. 8, p. 2923, 2022.

[12] F. Caccavale, P. Chiacchio, A. Marino, and L. Villani, "Six-dof impedance control of dual-arm cooperative manipulators," *IEEE/ASME Trans. On Mechatronics*, vol. 13, no. 5, pp. 576–586, 2008.

[13] F. Caccavale, G. Giglio, G. Muscio, and F. Pierri, "Cooperative impedance control for multiple uavs with a robotic arm," in *2015 IEEE/RSJ International Conference on Intelligent Robots and Systems (IROS)*. IEEE, 2015, pp. 2366–2371.

[14] F. Pierri, M. Nigro, G. Muscio, and F. Caccavale, "Cooperative manipulation of an unknown object via omnidirectional unmanned aerial vehicles," *Journal of Intelligent & Robotic Systems*, vol. 100, no. 3, pp. 1635–1649, 2020.

[15] F. Huzaefa and Y.-C. Liu, "Force distribution and estimation for cooperative transportation control on multiple unmanned ground vehicles," *IEEE Trans. on Cybernetics*, vol. 53, no. 2, pp. 1335–1347, 2021.

[16] A. Marino, "Distributed adaptive control of networked cooperative mobile manipulators," *IEEE Transactions on Control Systems Technology*, vol. 26, no. 5, pp. 1646–1660, 2017.

[17] A. Marino and F. Pierri, "A two stage approach for distributed cooperative manipulation of an unknown object without explicit communication and unknown number of robots," *Robotics and Autonomous Systems*, vol. 103, pp. 122–133, 2018.

[18] Z. Li, C. Yang, C.-Y. Su, S. Deng, F. Sun, and W. Zhang, "Decentralized fuzzy control of multiple cooperating robotic manipulators with impedance interaction," *IEEE Transactions on Fuzzy Systems*, vol. 23, no. 4, pp. 1044–1056, 2014.

[19] A. De Luca and R. Mattone, "Sensorless robot collision detection and hybrid force/motion control," in *Proceedings of the 2005 IEEE International Conference on Robotics and Automation*, 2005, pp. 999–1004.

[20] F. Caccavale and F. Pierri, "Distributed source-user estimation over directed graphs," *Automatica*, vol. 155, p. 111116, 2023.

[21] B. Siciliano, L. Sciavicco, L. Villani, and G. Oriolo, *Robotics – Modelling, Planning and Control*. London, UK: Springer, 2009.

[22] F. Caccavale and M. Uchiyama, *Cooperative Manipulators*. Berlin, Heidelberg: Springer Berlin Heidelberg, 2008, pp. 701–718.

[23] P. Chiacchio, S. Chiaverini, L. Sciavicco, and B. Siciliano, "Global task space manipulability ellipsoids for multiple-arm systems," *IEEE Trans. on Robotics and Automation*, vol. 7, no. 5, pp. 678–685, 1991.

[24] M. Sileo, Y. Karayiannidis, F. Pierri, and F. Caccavale, "Decentralized leader-follower control for centroid and formation tracking," in *2023 IEEE International Conference on Systems, Man, and Cybernetics (SMC)*. IEEE, 2023, pp. 3349–3354.

[25] J. Brewer, "Kronecker products and matrix calculus in system theory," *IEEE Trans. on Circuits and Systems*, vol. 25, no. 9, pp. 772–781, 1978.

[26] F. Caccavale and F. Pierri, "An approach to distributed estimation of time-varying signals by multi-agent systems," in *2022 IEEE 61st Conference on Decision and Control (CDC)*. IEEE, 2022, pp. 3556–3561.

[27] B. Siciliano, L. Sciavicco, L. Villani, and G. Oriolo, *Robotics: modelling, planning and control*. Springer Verlag, 2009.